







## Article

# Green Light Drives Embryonic Photosynthesis and Protein Accumulation in Cotyledons of Developing Pea (*Pisum sativum* L.) Seeds

Nataliia Stepanova <sup>1</sup>, Elena Tarakhovskaya <sup>2,3</sup> , Alena Soboleva <sup>4</sup>, Anastasia Orlova <sup>4</sup> , Aditi Basnet <sup>5</sup>, Anastasia Smolenskaya <sup>6</sup>, Nadezhda Frolova <sup>4</sup> , Tatiana Bilova <sup>2,4</sup>, Anastasia Kamionskaya <sup>1</sup> , Andrej Frolov <sup>4</sup>, Sergei Medvedev <sup>2</sup>  and Galina Smolikova <sup>2,\*</sup> 

- <sup>1</sup> Federal State Institution Federal Research Centre “Fundamentals of Biotechnology”, Russian Academy of Sciences, 119071 Moscow, Russia; stepanovanataliia.v@yandex.ru (N.S.); akamio@fbras.ru (A.K.)
  - <sup>2</sup> Department of Plant Physiology and Biochemistry, St. Petersburg State University, 199034 Saint Petersburg, Russia; elena.tarakhovskaya@gmail.com (E.T.); t.bilova@spbu.ru (T.B.); s.medvedev@spbu.ru (S.M.)
  - <sup>3</sup> Vavilov Institute of General Genetics, Saint Petersburg Branch, Russian Academy of Sciences, 199034 Saint Petersburg, Russia
  - <sup>4</sup> Laboratory of Analytical Biochemistry and Biotechnology, K.A. Timiryazev Institute of Plant Physiology, Russian Academy of Sciences, 127276 Moscow, Russia; orlova@ifr.moscow (A.O.); frolovanadja@yandex.ru (N.F.); afrolov0375@yandex.ru (A.F.)
  - <sup>5</sup> Faculty of Pharmacy, Martin-Luther University of Halle-Wittenberg, 06108 Halle, Germany; aditibasnet66@gmail.com
  - <sup>6</sup> Federal Research Center “N.I. Vavilov All-Russian Institute of Plant Genetic Resources”, 190031 Saint Petersburg, Russia; nastya-smolenska.n@yandex.ru
- \* Correspondence: g.smolikova@spbu.ru



**Citation:** Stepanova, N.; Tarakhovskaya, E.; Soboleva, A.; Orlova, A.; Basnet, A.; Smolenskaya, A.; Frolova, N.; Bilova, T.; Kamionskaya, A.; Frolov, A.; et al. Green Light Drives Embryonic Photosynthesis and Protein Accumulation in Cotyledons of Developing Pea (*Pisum sativum* L.) Seeds. *Agronomy* **2024**, *14*, 2367. <https://doi.org/10.3390/agronomy14102367>

Academic Editors: Sophie Brunel-Muguet and Guillaume Née

Received: 13 September 2024

Revised: 7 October 2024

Accepted: 11 October 2024

Published: 14 October 2024



**Copyright:** © 2024 by the authors. Licensee MDPI, Basel, Switzerland. This article is an open access article distributed under the terms and conditions of the Creative Commons Attribution (CC BY) license (<https://creativecommons.org/licenses/by/4.0/>).

**Abstract:** Photosynthesis is a vital process for seed productivity. It occurs in the leaves and provides developing seeds with the necessary nutrients. Moreover, many crops require photochemical reactions inside the seeds for proper development. The present study aimed to investigate *Pisum sativum* L. seeds at the middle stage of maturation, which is characterized by the active synthesis of nutrient reserves. Embryonic photosynthesis represents a crucial process to produce cells' NADP(H) and ATP, which are necessary to convert sucrose into reserve biopolymers. However, it remains unclear how the pea embryo, covered by a coat and pericarp, receives sufficient light to provide energy for photochemical reactions. Recent studies have demonstrated that the photosynthetically active radiation reaching the developing pea embryo has a high proportion of green light. In addition, green light can be utilized in foliar photosynthesis by plants cultivated in shaded conditions. Here, we addressed the role of green light in seed development. Pea plants were cultivated under red and blue (RB) LEDs or red, green, and blue (RGB) LEDs. A Chl *a* fluorescence transient based on OJIP kinetics was detected at the periphery of the cotyledons isolated from developing seeds. Our findings showed that the addition of green light resulted in an increase in photochemical activity. Furthermore, the mature seeds that developed in the RGB module had a significantly higher weight and more storage proteins. Using a metabolomics approach, we also detected significant differences in the levels of organic acids, carbohydrates, nucleotide monophosphates, and nitrogenous substances between the RB and RGB conditions. Under RGB light, the cotyledons contained more ornithine, tryptophan, arginine, and aspartic acid. These changes indicate an impact of green light on the ornithine–urea cycle and polyamine biosynthesis. These results allow for a deeper understanding of the photochemical processes in embryos of developing seeds grown under a low light intensity. The photosynthetic system in the embryo cell adapts to the shade conditions by using green light.

**Keywords:** *Pisum sativum* L.; seed; photosynthesis; green light; PAM fluorometry; metabolomics

## 1. Introduction

Over the last decade, the term “photosynthesis” has been extended beyond leaf photosynthesis to include other green plant parts [1–3]. The chlorophyll-containing embryos of some plants are no exception, suggesting that they are also capable of photosynthesis [4–7]. The presence or absence of chlorophyll in the embryo definitively classifies angiosperms into two categories: chloroembryophytes and leucoembryophytes [4,8]. The synthesis of chlorophyll in chloroembryos begins at the globular stage of embryogenesis and continues throughout the process, ceasing only at the late maturation stage when the seeds enter dormancy [9–11]. Furthermore, seeds contain carotenoids that participate in photosynthesis and act as abscisic acid (ABA) precursors [12,13]. Developing green seeds have photochemically active chloroplasts and are capable of producing assimilates that are further converted into reserve biopolymers [10,12,14–18]. The dark reactions of photosynthesis in developing seeds are characterized by the fact that the main source of carbon is sucrose derived from the parent plant [4,12]. Consequently, embryonic chloroplasts primarily function to produce NADP(H) and ATP, which are then used to convert sucrose to acetyl-CoA and, subsequently, to fatty acids and triacylglycerides [12,19,20]. In addition, oxygen is released during photosynthesis, preventing hypoxia and maintaining seed respiration [21,22]. However, the question of how the seed embryo, covered by a pericarp and coat, receives enough light to provide energy for photochemical reactions remains unresolved.

Recently, we studied how light transmits through the different green tissues of pea (*Pisum sativum* L.) plants [23]. On average, a photochemically active green leaf transmits only about 15% of the photosynthetically active radiation (PAR), with about 5% being red light and no blue light. PAR passing through the pod-covering tissues (pericarp and coat) also showed no blue light and a low amount of red light (about 2%). However, in the spectrum of light reaching the cotyledons of developing pea seeds, a high proportion of green and far-red light was found. Nevertheless, regardless of low irradiance and spectral regions not typical for leaf photosynthesis, cotyledons demonstrated photochemical activity, as measured by pulse-amplitude-modulated (PAM) fluorometry. To explain this phenomenon, we need to take a closer look at green light.

Green light has long been thought to be of little importance in plant biology. There is a widespread historical misconception that green light is not efficiently used in photosynthesis because chlorophylls have minimal absorption in the green band of light. However, this idea, first proposed by Frits Went in 1957 [24], has not been confirmed experimentally. Recent studies suggest that green light can be absorbed by plant leaves and may be involved in the regulation of various physiological responses such as stomata movement, shadow avoidance, photomorphogenesis, and photosynthesis [25–29]. Blue and red light are primarily absorbed and utilized by the superficial cells of the columnar mesophyll, while green light can penetrate deeper (into the leaf and/or canopy) and drive leaf photosynthesis in combination with other light sources, especially in strong white light [26,30–32]. This is believed to explain the phenomenon of why the addition of green light-emitting diodes (LEDs) to red and blue ones increases the productivity of various plants grown under artificial lighting in greenhouses [33–36].

The addition of green light has been shown to affect leaf photochemical efficiency in *Helianthus annuus* L. [37], *Lactuca sativa* [38–40], *Cucumis sativus* [41,42] *Solanum lycopersicum* L. [27], *Zingiber officinale* Roscoe [28], *Triticum aestivum* [43], and *Coleus* [44]. According to Terashima et al. [37], leaves can increase the absorption of PAR and drive photosynthesis in the chloroplasts of all mesophyll layers by using chlorophylls that weakly absorb green light. In tomato plants, adding up to 30% green light to the blue and red spectrum was shown to have mostly beneficial effects, but 40% green light induced shade avoidance [27]. On the other hand, the addition of green light under moderate to intense white light illumination is more effective in stimulating photosynthesis than the addition of red light [37]. Intense green light did not induce the accumulation of reactive oxygen species that usually occurs under light stress caused by red light [28].

We suggest that green light can contribute significantly to so-called non-foliar photosynthesis. Green plant organs such as petioles, stems, inner bark, fruits, and pods are known to synthesize chlorophylls and develop active chloroplasts [2,3,5,6,17]. Most of them acquire photochemical reactions under low amounts of blue and red light and with a high amount of irradiation in the range of 500–600 nm. However, this effect has not yet been studied.

The object of our study was pea (*Pisum sativum* L.) seeds. Pea is a member of the Leguminosae family, which plays an important role in global agriculture, accounting for approximately 27% of the world's crop production [45]. Pea seeds are a rich source of nutrients, comprising protein, starch, soluble sugars, fiber, and a range of minerals and vitamins. They are particularly abundant in protein, making them a valuable component of animal feed and human nutrition [46]. Ensuring the quality of pea seeds is, therefore, a crucial aspect of sustainable agricultural practices and efficient nutrition.

This study aimed to understand the role of green light in the photochemical processes occurring in the embryos of developing pea seeds. The novelty lies in the comparison of the photochemical activity, quality, and biochemical composition of seeds developed under different light spectra (red and blue LEDs vs. red, green, and blue LEDs). We show how green light affects pea seed maturation. These results will allow for a deeper understanding of the photochemical processes in embryos of developing seeds grown under a low light intensity.

## 2. Materials and Methods

### 2.1. Reagents

The reagents were purchased from the following manufacturers: Conlac GmbH (Leipzig, Germany)—hexane (puriss p. a.); Macherey-Nagel GmbH and Co KG (Düren, Germany)—N-methyl-N-(trimethylsilyl)trifluoroacetamide (MSTFA, MS grade); Reanal (Budapest, Hungary)—L-aspartic acid and 2-oxoglutaric acid; Vekton (Saint-Petersburg, Russia)—methanol (LC grade). All other chemicals were purchased from Sigma-Aldrich Chemie GmbH (Taufkirchen, Germany). Water was purified in house with a water conditioning and purification system (Millipore Milli-Q Gradient A10 system; resistance 18 mΩ/cm; Merck Millipore, Darmstadt, Germany).

### 2.2. Plant Material and Growth Conditions

The plants were grown in 2024 in an experimental climate control facility at the Institute of Bioengineering (Research Center of Biotechnology, Russian Academy of Sciences) under a constant air temperature of  $24 \pm 2$  °C and 16 h photoperiod. Commercial seeds of pea (*Pisum sativum* L.) of the vegetable cv. Gloria were germinated at  $23 \pm 1$  °C between layers of moist filter paper until visible radicle protrusion occurred and were then transferred to 2 L pots (five seedlings per pot) filled with soil (All-Mix BioBizz substrate, Biobizz Worldwide Organics, Drachten, The Netherlands). The growth chamber included RB and RGB modules (three pots per module). The *RB module* was illuminated with red LEDs (RL, 600–700 nm, maxima of 660 nm,  $165 \pm 17$  μmol photons m<sup>-2</sup> s<sup>-1</sup>) and blue LEDs (BL, 400–500 nm, maxima of 450 nm,  $42 \pm 4$  μmol photons m<sup>-2</sup> s<sup>-1</sup>) (Figure S1a,c). The *RGB module* was illuminated with red LEDs (RL, 600–700 nm, maxima of 660 nm,  $155 \pm 17$  μmol photons m<sup>-2</sup> s<sup>-1</sup>), blue LEDs (BL, 400–500 nm, maxima of 450 nm,  $44 \pm 4$  μmol photons m<sup>-2</sup> s<sup>-1</sup>), and green LEDs (GL, 500–600 nm, maxima of 520 nm,  $32 \pm 3$  μmol photons m<sup>-2</sup> s<sup>-1</sup>) (Figure S1b,d). The spectral characteristics of the light sources were measured using a UPRtek PG100N spectroradiometer (Taiwan, China). The seeds were harvested at the middle maturation stage and after late maturation.

### 2.3. Evaluation of Seed Germination and Seedling Development

The germination capability of the mature pea seeds was determined. Four replicates of ten seeds were incubated between wet filter papers at  $23 \pm 1$  °C. To measure the rate of germination, the number of germinated seeds was counted daily over a period of eight days.

Seeds were considered germinated when visible radicle protrusion occurred. The times required for 10, 25, and 50% germination ( $T_{10}$ ,  $T_{25}$ , and  $T_{50}$ , respectively) were calculated using the formulae proposed by Coolbear et al. [47]. The total germination percentage (GP) was calculated as the number of germinated seeds divided by the total number of seeds. The percentage of normally developed seedlings (NSP) was calculated according to the ISTA rules [48,49].

#### 2.4. Estimation of Protein, Starch, and Oil Contents

For the determination of the total protein, starch, and oil contents, pea cotyledons were isolated from mature pea seeds, lyophilized, and ground into a fine powder. The data are presented as the mean  $\pm$  standard deviation (SD) of three replicates ( $n = 3$ ).

Total protein was determined using the Kjeldahl method using a nitrogen-to-protein conversion factor of 6.25 [50,51]. Samples (300 mg) were heated at 420 °C for 1.5 h with 5 mL of concentrated sulfuric acid, which digests the organic substances through oxidation to release the reduced nitrogen. Calcium carbonate was added as a catalyst to increase the boiling point of the sulfuric acid. Subsequently, the sample solution was distilled in a hot 33% alkaline solution of sodium hydroxide ( $v/v$ ) with the addition of distilled water and 3% boric acid ( $v/v$ ). The amount of nitrogen in the sample (ammonium ion concentration) was measured using a VELP UDK 159 protein analyzer (Velp Scientifica, Usmate, Italy) using automatic titration of a 0.1 N sulfuric acid solution.

The starch contents were determined using the Ewer's polarimetric method and a conversion factor of an angle of rotation of starch of 174.7 [50]. The samples (1.5 g) were hydrolyzed in 25 mL of 1% ( $v/v$ ) hydrochloric acid for 15 min in a boiling water bath under continuous shaking at an amplitude of 30 mm and a frequency of 150 rpm and then cooled to room temperature. To precipitate opalescent substances (polysaccharides, proteins, and other biopolymers), 10% ( $v/v$ ) phosphoric acid (2.5 mL) was added. After filtration, the optical rotation in the supernatants was determined using an automatic SACI polarimeter (ATAGO, Japan).

The total lipid contents were determined using the method of Ermakov and co-workers, based on Soxhlet extraction [50]. To secure the complete removal of water, the previously dried samples were placed in 9  $\times$  9 filter paper envelopes and incubated in a thermostat at 100 °C for 3 h. Then, the envelopes were placed in the extractor of the Soxlet apparatus (EFLAB EFSOX-6, Moscow, Russia) filled 2/3 full of petroleum ether. After 12 h, the oil extraction was stopped, the envelopes were dried at 105 °C for 1.5 h, cooled in a desiccator in closed Petri dishes, and weighed.

#### 2.5. Chlorophyll *a* Fluorescence

The kinetics of chlorophyll (Chl) *a* fluorescence OJIP was determined using a PAR-FluorPen FP 110 fluorometer (Photon Systems Instruments, Drasov, Czech Republic) according to the manufacturer's protocol [52]. The device was equipped with saturating, actinic, and measuring light sources with an emission maximum of 455 nm and fluorescence detection at wavelengths of 667–750 nm. Cotyledons ( $n = 6$ ) were isolated from the pea seeds at the mid-maturation stage, placed on moist filter paper (to prevent drying), and kept in light-proof boxes for 30 min for dark adaptation. Afterwards, they were exposed to a blue pulse of 2400  $\mu\text{mol photons m}^{-2} \text{s}^{-1}$ , and the minimum ( $F_0$ ) and maximum ( $F_m$ ) values of Chl *a* fluorescence were detected. The measured parameters were used to estimate the photochemical activity of photosystem II (PSII) according to the method described by Strasser et al. [53]. The estimated values are shown in Table 1.

**Table 1.** Formulas and definitions of OJIP-test parameters (according to [53]).

Value	Formula	Definition
PI <sub>ABS</sub>	$(RC/ABS) \cdot (TR_O/DI_O) \cdot [ET_O/(TR_O - ET_O)]$	Photosynthetic performance index based on absorption
PHI <sub>Po</sub>	$1 - [(F_m - F_o)/F_m]$	Maximum quantum yield of primary photochemistry
PHI <sub>Eo</sub>	$[1 - (F_o/F_m)] \cdot (1 - V_j)$	Overall electron transport potential of the active RC
PHI <sub>Do</sub>	$1 - PHI_{Po}$	Potential energy dissipation flux
ABS/RC	$M_O \cdot (1/V_j) \cdot (1/Phi_{Po})$	Specific light absorption flux per RC
TR <sub>O</sub> /RC	$M_O \cdot (1/V_j)$	Captured energy flow per RC
ET <sub>O</sub> /RC	$M_O \cdot (1/V_j) \cdot (1 - V_j)$	Electron transport flow per RC
DI <sub>O</sub> /RC	$(ABS/C) - (TR_O/RC)$	Energy dissipation flux per RC

RC—reaction center; ABS—absorption; F<sub>O</sub>—minimal fluorescence intensity; F<sub>m</sub>—maximal fluorescence intensity; V<sub>j</sub>—relative variable fluorescence at the J step of OJIP curve; M<sub>O</sub>—initial slope of relative variable fluorescence.

### 2.6. Analysis of Thermally Stable Polar Metabolites

The analysis of thermally stable polar (and mainly primary) metabolites relied on a two-step aqueous methanol extraction of frozen homogenized pea cotyledons (20 ± 2 mg FW), performed as described in [54] with minor modifications. Adonitol (50 µmol/L) was supplemented as an internal standard (IS) to the extractant (methanol) prior to the extraction procedure. Aliquots (80 µL) of the extracts were evaporated to dryness at 4 °C using a Labconco CentriVap vacuum concentrator (Labconco Corporation, Kansas City, MO, USA). The specified volume of the sample aliquots was optimized for subsequent derivatization and gas chromatography–mass spectrometry (GC-MS) analysis in a series of preliminary experiments. The obtained dry residues were sequentially derivatized with methoxyamine hydrochloride (MEOX) and *N*-methyl-*N*-(trimethylsilyl)trifluoroacetamide (MSTFA), according to a previously established procedure [55].

The samples (1 µL) were analyzed by gas chromatography–electron ionization–quadrupole mass spectrometry (GC-EI-Q-MS) using a GC2010 gas chromatograph coupled online to a Shimadzu GCMS QP2010 quadrupole mass selective detector equipped with a CTC GC PAL liquid injector (Shimadzu Deutschland GmbH, Duisburg, Germany) under the instrumental settings summarized in Table S1.

A sequence for the GC-MS analysis included samples of different types arranged in the following order: (i) hexane, (ii) a mix of C10–C40 alkanes dissolved in hexane, (iii) MSTFA, (iv) the derivatization blank (blank, containing only derivatizing agents), (v) the extraction blank (containing only IS and derivatizing agents), (vi) the experimental samples in random order, (vii) quality controls (QC) prepared from aliquots of the pooled individual extracts, and (viii) 28 mixes of 4–6 authentic standards (50 µmol/L for each compound). The QC samples were analyzed after every 5–6 experimental samples and then used to assess the method performance and to control for within-group variation in the analytes.

Processing of the acquired GC-MS data relied on an untargeted approach, which performed unbiased annotation of all the detected total ion current (TIC) chromatographic peaks. For this, the TIC peak annotation with a specific metabolite feature relied on matching the feature-specific retention time (*t<sub>R</sub>*) maxima of at least three characteristic extracted ion chromatograms (XICs, *m/z* ± 0.5 Da) with a signal-to-noise ratio (S/N) ≥ 3. The peak annotation was performed using the Automated Mass Spectral Deconvolution and Identification System (AMDIS, version 2.66 (08.08.2008), freely available at [www.amdis.net](http://www.amdis.net), accessed on 9 March 2024) and Xcalibur, version 3.0.63 (05.08.2013) (ThermoFisher Scientific Inc., Bremen, Germany). Kovats retention time indices (RIs) were calculated from the retention times of alkane C10–C40 standards (Table S2). The metabolite annotations were based on available spectral libraries—the National Institute of Standards and Technology (NIST), the Golm Metabolome Database (GMD), and the in-house Authentic Standard Library (ASL). The quantitation was based on integrating the corresponding extracted ion chromatograms (XICs, *m/z* ± 0.5 Da) at specific retention times (*t<sub>R</sub>*).



### 2.7. Analysis of Thermally Labile Polar Metabolites

Thermally labile anionic polar metabolites were analyzed using reversed phase ion-pair ultra-high performance liquid chromatography–electrospray ionization–triple quadrupole tandem mass spectrometry (RP-IP-UHPLC-ESI-QqQ-MS/MS), following the method described in [56] with minor modifications. In detail, the frozen pea cotyledons were homogenized and  $100 \pm 5$  mg FW was transferred into pre-cooled 2 mL polypropylene microtubes with 200 mg of glass beads (0.75–1 mm diameter), 3 stainless steel beads (3 mm diameter), and 1 stainless steel bead (5 mm diameter). The material was extracted through a two-step procedure. The first step used 900  $\mu$ L of an ice-cold ( $-80$  °C) mixture of dichloromethane/ethanol (2:1, *v/v*) and 100  $\mu$ L of ice-cold HCl/water (1:200, *v/v*). The mixture was intensively homogenized (5.0 m/s,  $3 \times 20$  s; FastPrep-24TM, MP Biomedicals, Eschwege, Germany). After the subsequent centrifugation (4 °C,  $10,000 \times g$ , 5 min), the polar supernatant fraction (300  $\mu$ L) was collected into a new pre-cooled 1.5 mL microtube. During the second extraction step, the plant material residue was resuspended in an additional portion (50  $\mu$ L) of ice-cold HCl/water (1:200, *v/v*). After vortexing (30 s, 500 rpm) and centrifugation (4 °C,  $10,000 \times g$ , 5 min) of the samples, the resulting polar supernatant fraction (120  $\mu$ L) was combined with the first portion of the polar extract. The combined extracts were further centrifuged ( $10,000 \times g$ , 4 °C, 10 min), the supernatants were transferred to glass inserts of chromatographic vials, and sealed with membrane-attached plastic septa. Aliquots (5  $\mu$ L) of the extracts were analyzed using a Waters ACQUITY H-Class UPLC system (Waters GmbH, Eschborn, Germany) coupled online to an AB Sciex QTRAP 6500 MS/MS system (AB Sciex, Darmstadt, Germany) and the chromatographic and mass spectrometric settings presented in Table S3. A sequence for the UHPLC-MS analysis included samples of various types: experimental samples in random order, QC samples, multicomponent standard solution samples, and extraction blanks. Targeted acquisition of UHPLC-MS data was performed in the multiple reaction monitoring (MRM) mode and based on characteristic combinations of Q1 and Q3 mass ranges (MRM transitions) of 157 individual authentic standards representing the target compounds. For quantitative analysis, the extracted MRM chromatograms were integrated at specified  $t_{RS}$  using the MultiQuan<sup>TM</sup> software (version 3.0.2, AB Sciex, Darmstadt, Germany).

Both the GC-MS and UHPLC-MS datasets were checked for technical issues that might affect data acquisition. To validate the high quality of the acquisition performed, the datasets, each including experimental samples and QCs, were analyzed by PCA (Figure S3). In both cases, the PCA score plots built for the QCs in the coordinates of the two first principal components (PCs) showed relatively low intra-group variability. This confirms that there were no technical problems with the datasets, and they can be further analyzed.

### 2.8. Statistical Analysis

Statistical analysis of the seed quality parameters and photosynthetic performance parameters was accomplished using JASP (version 0.18.3) software (<https://jasp-stats.org>, accessed on 15 April 2024). The data are presented as the mean  $\pm$  SD, and the significance of differences between groups was estimated using Student's *t*-test.

The integrated areas of the metabolite peaks detected by both the GC-MS and UHPLC-MS analyses were combined, FW-normalized, and filtered to exclude the analytes absent in more than 20% of the samples and those showing high variation ( $RSD \geq 30\%$ ) in the quality control (QC) samples. The resulting dataset was processed and statistically interpreted using the MetaboAnalyst 6.0 online platform ([www.metaboanalyst.ca](http://www.metaboanalyst.ca), accessed on 10 April 2024). The quantitative data of the combined GC-MS and LC-MS-based metabolomics analyses were analyzed by principal component analysis (PCA) and hierarchical clustering analysis with a heatmap representation to visualize the changes in the level of each assigned metabolite and with a volcano plot representation. The univariate statistics results are presented as the mean  $\pm$  SD of five biological replicates. Fold changes (FCs) in the abundance of individual metabolites and significance of differences (*p*-value) between the compared groups were estimated using Student's *t*-test. The threshold values for the FCs

and  $p$ -values presented in the tables and figures were 1.5 and 0.05, respectively. To assess the reliability of the FC in the relative levels of individual metabolites, false discovery rates (FDRs) at  $p \leq 0.05$  were estimated for all comparisons using the Benjamini–Hochberg method [57].

### 3. Results

To understand the effect of green light on the maturation peculiarities of *P. sativum* seeds in the RB and RGB modules, we initially studied their photosynthetic performance during development in the mother plants. Seeds at the mid-maturation stage were selected for analysis (Figure 1).



**Figure 1.** Images of *P. sativum* pod (left) and seed (right) at the middle stage of maturation (in longitudinal section): Pr—pericarp; C—coat; Ct—cotyledon; Ax—axis including root, hypocotyl, epicotile, and plumule.

#### 3.1. Photosynthetic Performance Index, Flux Ratio, and Specific Fluxes (OJIP Test) of the Cotyledons of Pea Seeds at the Middle Stage of Maturation

The OJIP curve typically exhibits three distinct plateaus, each corresponding to a specific step in the electron transfer process within the electron transport chain of chloroplasts. Following the application of actinic light, the intensity of the chlorophyll fluorescence increases from the initial value ( $F_0$ ) to the maximum ( $F_m$ ) through two intermediate phases ('J' and 'I').  $F_0$  is regarded as the point at which the reaction centers (RCs) of photosystem II (PSII) are open.  $F_m$  is the excitation level that saturates the RCs with electrons. Based on the transient of Chl *a* fluorescence, the different parameters of photochemical activity were calculated at the periphery of cotyledons isolated from developing seeds (Figure 2).

The photosynthetic performance index ( $PI_{ABS}$ ) was used to estimate the overall photosynthetic efficiency, where ABS represents the photon flux absorbed by the chlorophylls in the antenna complex.  $PI_{ABS}$  is related to the density of active RCs, ratio of trapping flux, and ratio of dissipation flux. Therefore, it includes the whole energy cascade from the absorption of photons to plastoquinone (PQ) pool reduction.

The maximum quantum yield of primary photochemistry ( $PHI_{P_0}$ ) and the probability of a trapped exciton to move an electron into the electron transport chain ( $PHI_{E_0}$ ) reflect the overall photosynthetic and electron transport potential of the active RCs in PSII.  $PHI_{P_0}$  and  $PHI_{E_0}$  were 1.2 and 1.3 times higher, respectively, at the periphery of cotyledons developed under added green light (Figure 2a,b). No notable discrepancies in the  $TR_0/RC$  (trapping of excitons per active RC) and in  $ET_0/RC$  (electron transport flux per RC beyond  $Q_A$ ) were observed between the cotyledons developed in the RB and RGB modules (Figure 2c and 2d, respectively).  $PHI_{D_0}$  and  $DI_0/RC$ , which reflect the non-photochemical dissipation flux per reaction center, were found to be 1.2 and 1.4 times lower, respectively (Figure 2e,f). The combined effect of these factors was a doubling of the  $PI_{ABS}$  value in cotyledons developed under green light, indicating a significant increase in their photosynthetic activity (Figure 2g).

We detected a 1.3-time decrease in the value of  $ABS/RC$  in cotyledons developed in the RGB module, which suggests a reduction in the effective antenna size under green light (Figure 2h).

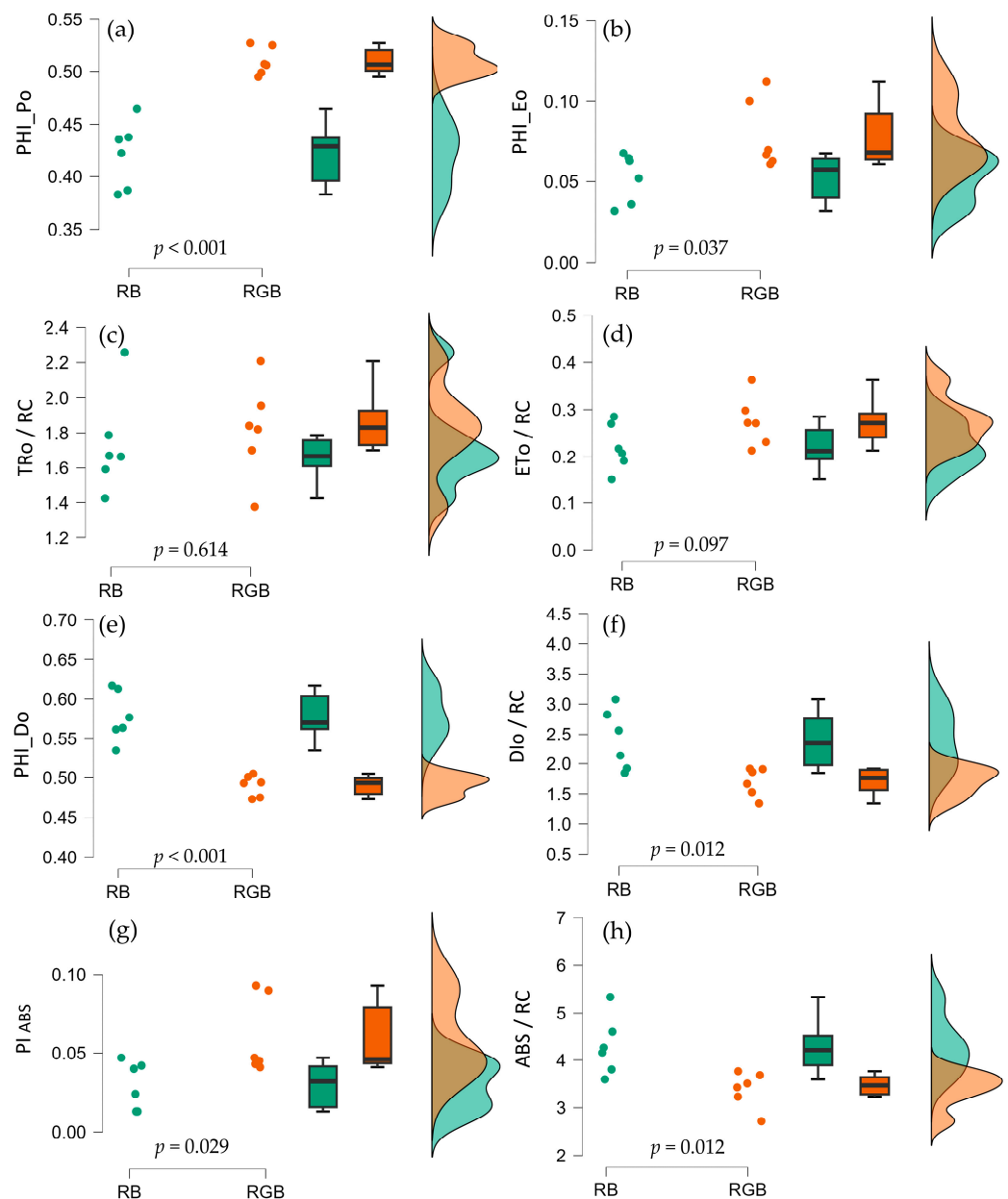


**Figure 2.** Raincloud plots shown photosynthetic performance in cotyledons of developing pea seeds at middle maturation stage: RB—red and blue illumination; RGB—red, green, and blue illumination. (a) PHI<sub>PO</sub>—the overall quantum yield of primary photochemistry; (b) PHI<sub>EO</sub>—the quantum yield of electron transport; (c) TR<sub>O</sub>/RC—the captured energy flow per reaction center; (d) ET<sub>O</sub>/RC—the electron transport flow per reaction center; (e) PHI<sub>DO</sub>—the potential energy dissipation flux at the level of the antenna complex chlorophylls; (f) DI<sub>O</sub>/RC—the specific energy dissipation flux at the level of the antenna complex chlorophylls; (g) PI<sub>ABS</sub>—the photosynthetic performance index, which includes energy cascade processes from the first absorption events to PQ reduction; (h) ABS/RC—the specific light absorption flux per reaction center. Plots display the individual cases (colored dots), box plots, and densities for each group. The x-axis and colors represent the grouping variable, and the y-axis represents the photosynthetic performance variable (rel. units). Within the box plots, the bold black line shows the sample median, the hinges indicate the 25th and 75th quantiles, and the whiskers point to 1.5 interquartile ranges beyond the hinges. Densities were estimated using a Gaussian kernel and the bandwidth was determined using the ‘nrd0’ method [58].



### 3.2. Germination Performance and Biochemical Composition of Mature Pea Seeds Developed under Different Light Conditions

In the next step, we compared the quality of the mature seeds developed in RB (red–blue) and RGB (red–green–blue) modules in terms of their germination performance and nutritional value. Overall, the seeds developed in the RGB module in the presence of green light had significantly higher weights than those developed in the RB module under blue and red light only (Table 2). The seed weight in the RGB module was 7.6% higher than that observed in the RB module.

**Table 2.** Quality (weight, germination) and biochemical composition (proteins, starch, oils) of *P. sativum* mature seeds developed in RB and RGB modules: GP—germination percentage; NSP—normal seedling percentage; T<sub>10</sub>, T<sub>25</sub>, and T<sub>50</sub>—time to 10, 25, and 50% germination, respectively.

Parameter	Module	Mean	SD	Student's <i>t</i> -Test			
				<i>t</i>	df	<i>p</i> -Value	Cohen's <i>d</i>
Weight, g	RB	0.234	0.035	−15.205	58	<0.001	−1.979
	RGB	0.251	0.036				
Proteins, %	RB	19	0.2	−7.913	4	0.001	−6.461
	RGB	22	0.6				
Starch, %	RB	50	0.8	−0.393	4	0.714	−0.321
	RGB	51	1.6				
Oils, %	RB	13	1.1	−0.427	4	0.691	−0.349
	RGB	14	0.5				
GP, %	RB	94	6.9	0	6	1.000	0
	RGB	94	6.9				
T <sub>10</sub> , days	RB	1.7	0.5	1.819	6	0.119 <sup>A</sup>	1.286
	RGB	1.3	0.1				
T <sub>25</sub> , days	RB	2.0	0.4	1.437	6	0.201 <sup>A</sup>	1.016
	RGB	1.6	0.2				
T <sub>50</sub> , days	RB	2.6	0.1	1.895	6	0.107 <sup>A</sup>	1.340
	RGB	2.2	0.4				
NSP, %	RB	73	19.2	−1.866	6	0.111 <sup>A</sup>	−1.319
	RGB	91	5.9				

SD—standard deviation of the mean ( $n = 4$ ); *t*—value of *t*-statistic; df—degree of freedom; Cohen's *d*—effect size for Student's *t*-test (using the pooled standard deviation to standardize the mean difference). <sup>A</sup> Brown–Forsythe test is significant ( $p < 0.05$ ), suggesting a violation of the equal variance assumption.

The total percentage of germinated seeds (GP) showed no difference between the seeds developed in the RB and RGB modules (Table 2). The value was 94% for both modules. The seeds developed in the RGB module had lower values of T<sub>10</sub>, T<sub>25</sub>, and T<sub>50</sub>, which indicates a higher germination rate. There was also a higher percentage of normal seedlings (NSP) with well-developed essential structures. However, the differences in the germination performance parameters were not statistically significant.

To address the nutritional value, we determined the contents of proteins, starch, and oils in the mature pea seeds developed in the RB and RGB modules. No differences in starch and oil contents (as %DW) were observed (Table 2). However, the total protein contents were significantly different (with *p*-value = 0.01 and Cohen's *d* value = 6.461). The protein content of embryos developed in the RGB module was 15.8% higher than that of embryos grown in the RB module.

### 3.3. Metabolomics Analysis of Mature Pea Seeds Developed under Different Light Conditions

To investigate the potential metabolic pathways underlying the effect of RGB light on seed quality, we characterized the biochemical composition of cotyledons isolated from mature *P. sativum* seeds developed in the RB and RGB modules. The biochemical analysis was based on a combined GC-MS and UHPLC-MS approach.

The GC-MS-based metabolite profiling of the cotyledons revealed 143 individual trimethylsilyl (TMS) and MEOX-TMS derivatives, of which, 68 analytes were identified

based on co-elution with authentic standards, RI values, and spectral similarity, and 60 analytes were structurally annotated based on their RI values and spectral similarity to MS library data (Table S4). The thermally stable low-molecular-weight metabolites were represented by the following chemical classes: 17 amino acids, including 5 non-proteinogenic ones ( $\beta$ -alanine, homoserine, ornithine,  $\gamma$ -aminobutyric acid, and pyroglutamic acid); 14 organic acids (di- and tricarboxylic acids of the tricarboxylic acid (TCA) cycle, glycolic acid, tartaric acid, several derivatives of butyric acid, etc.); 40 carbohydrates (mono-, di-, and trisaccharides, sugar phosphates, polyols, and aldonic acids); four phenolic compounds, including three phenolic acids; five fatty acids (palmitic, linoleic, oleic, etc.); four amines, including the polyamines putrescine and spermidine; two sterols (campesterol and sitosterol); and a miscellaneous group of metabolites (Table S4). The other 34 analytes could not be attributed to certain structures but were successfully annotated to specific chemical classes due to the presence of characteristic fragment ions ( $m/z \pm 0.5$ ) in their EI mass spectra. The following  $m/z$  values of the fragment ions were used according to Harvey and Vouros [59]: 100 and 174—amino group-containing metabolites; 299, 315, 357, or /and 387—phosphate group-containing compounds; 103, 160, 217, and 319—C6 monosaccharides; 204 and 319—sugar alcohols, 318 and 319—stereoisomers of inositol; 292, 333, and 319—sugar-derived acids; 361, 437, or /and 451—di- and trisaccharides. The analytes that could not be unambiguously annotated were marked as unknown.

The targeted UHPLC-MS analysis revealed 88 thermally labile metabolites, annotated by co-elution with authentic standards and MS data (Table S5): 14 sugar phosphates and their derivatives, 35 nucleotides and nucleosides, 16 amino acids, 18 organic acids, pantothenic acid, glutathione, allantoin, etc. Most of the amino acids, several organic acids (citric, malic, glycolic, and fumaric acids), glucose, sucrose, and several sugar phosphates were detected by both analytical approaches (GC-MS and UHPLC-MS).

Thus, 231 thermally stable and thermally labile metabolites representing carbohydrates, amino acids, organic acids, phenolic acids, fatty acids, amines, and sterols were annotated (Tables S4 and S5). These metabolites were used in a principal component analysis (PCA) to discriminate the difference in biochemical composition between seeds developed under different supplemental lighting conditions.

The first two principal components (PC1 and PC2) showed a clear clustering of the pea cotyledons developed in the RB and RGB modules (Figure 3a). PC1 explained 71.9% of the total variation and PC2 explained 19.2%, together covering up to 91.1% of the total variance. Notably, the RGB group had higher inter-group variance.

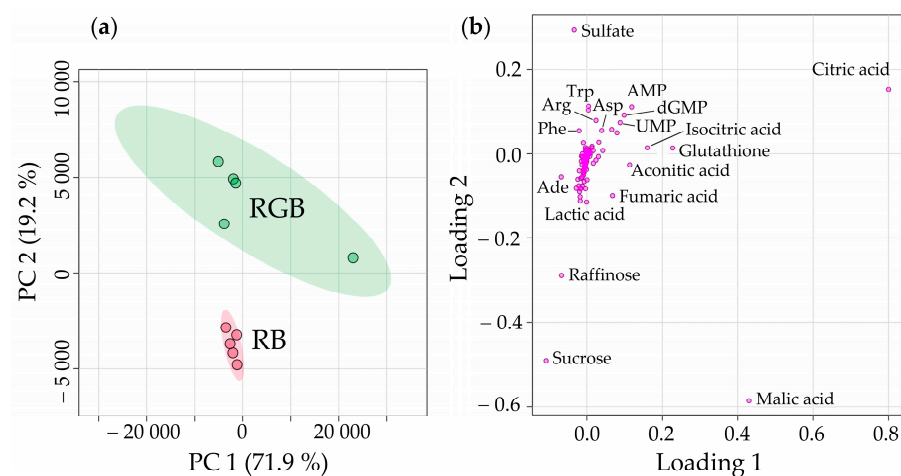


**Figure 3.** Sample scores (a) and loading plot (b) for the first two principal components derived from PCA of the thermostable and thermolabile polar metabolite profiles of *P. sativum* cotyledons isolated from mature seeds developed under red–blue (RB) and red–green–blue (RGB) light. AMP—adenosine monophosphate; dGMP—2-deoxyguanosine-5-monophosphate; UMP—uridine monophosphate; Phe—phenylalanine; Arg—arginine; Asp—aspartic acid; Trp—tryptophan.

The metabolites with the highest loadings (i.e., the strongest contributors to the inter-sample differences presented in the score plot) included organic acids of the TCA cycle (citric, malic, and aconitic acids), lactic acid, sucrose, raffinose, sulfate, several amino acids (Arg, Trp, Asp, and Phe), glutathione, adenosine (Ade), and nucleotide monophosphates (AMP, dGMP, and UMP) (Figure 3b).

At the next step, a volcano plot was generated to select specific compounds with the highest and most reliable contribution to the green light-dependent changes in the metabolite profiles of pea cotyledons (Figure S4). The list of 52 metabolites with significantly different abundances is presented in Table 2 ( $p < 0.05$ ,  $FC \geq 1.5$ ). Most of the metabolites showed a decrease in abundance (up to 8-fold) in the cotyledons developed under RGB light compared to those developed under RB light (Figure 3b, Table 3). Among them, carbohydrates (sugars, polyols, and sugar acids), organic acids, and nitrogen-containing substances (uric acid, spermidine, and several cyclic nucleotides) were the dominant ones. Uric acid, lactic acid, and  $\alpha$ -ketoglutaric acid showed the most dramatic (3.4–7.6-fold) decrease in relative contents. Surprisingly, only four amino acids were significantly up-regulated under RBG light: ornithine, tryptophan, arginine, and aspartic acid (Table 3).

**Table 3.** Green light-regulated metabolites of cotyledons isolated from the mature *P. sativum* seeds. The table includes compounds with significantly ( $p < 0.05$ , FDR-adjusted) differing abundances under the tested experimental conditions (RB light vs. RGB light) with a fold change  $\geq 1.5$ . The statistical analysis was performed using MetaboAnalyst 6.0 (<http://www.metaboanalyst.ca>, accessed on 10 April 2024).

Metabolite	Fold Change	Adjusted $p$ -Value	Analysis Method
<b>Down-Regulated Metabolites</b>			
Organic acids:			
Lactic acid	5.9, 4.3	<0.001, <0.001	GC-MS, LC-MS
$\alpha$ -Ketoglutaric acid	3.3, 2.4	0.027, <0.001	GC-MS, LC-MS
2-Hydroxyglutaric acid	2.9	<0.001	GC-MS
2,4-Hydroxybutyric acid	2.8	0.002	GC-MS
Tartaric acid	2.3	0.036	GC-MS
Glycolic acid	1.9	0.004	GC-MS
Malic acid	1.8	<0.001	GC-MS
$\gamma$ -Aminobutyric acid	1.7	<0.001	GC-MS
$\beta$ -Hydroxybutyric acid	1.6	0.003	GC-MS
Pyruvic acid	1.5	0.005	LC-MS
Sugars, sugar-phosphates, polyols, sugar acids:			
Maltose	3.3	0.001	GC-MS
Dulcitol	2.6	<0.001	GC-MS
Xylitol	2.5	<0.001	GC-MS
Maltitol	2.4	<0.001	GC-MS
RI 3460 trisaccharide	2.1	<0.001	GC-MS
RI 3502 trisaccharide	2.1	<0.001	GC-MS
Sequoitol	2.0	<0.001	GC-MS
RI 3487 trisaccharide	2.0	<0.001	GC-MS
Erlose	1.9	<0.001	GC-MS
RI 2687 carbohydrate	1.9	<0.001	GC-MS
Galactonic acid	1.9	<0.001	GC-MS
Glyceraldehyde-3-phosphate	1.8	0.033	LC-MS
Xylose	1.7	0.001	GC-MS
RI 2719 disaccharide	1.7	<0.001	GC-MS
Galactose	1.7	0.002	GC-MS
Glucaric acid	1.6	<0.001	GC-MS
Glycerol-3-phosphate	1.6	0.002	LC-MS
Galactaric acid	1.6	0.013	GC-MS
Glucuronic acid	1.6	0.002	GC-MS

Table 3. Cont.

Metabolite	Fold Change	Adjusted <i>p</i> -Value	Analysis Method
<b>Down-Regulated Metabolites</b>			
RI 2183 hexose	1.6	<0.001	GC-MS
Mannose	1.5	0.004	GC-MS
Sucrose	1.5	<0.001	GC-MS
N-containing metabolites:			
Uric acid	7.1	<0.001	LC-MS
Spermidine	1.9	0.008	GC-MS
Nicotinic acid	1.8	<0.001	LC-MS
RI 2487 amine	1.8	0.030	GC-MS
Glutamic acid	1.8	<0.001	GC-MS
Ethanolamine	1.5	0.004	GC-MS
Nucleotides:			
Cyclic guanosine monophosphate	2.1	0.006	LC-MS
Adenosine-2,3-cyclic monophosphate/adenosine-3,5-cyclic monophosphate	1.8	0.004	LC-MS
Miscellaneous and unknowns:			
Pentanoic acid derivative	2.0	0.016	LC-MS
Methylphosphate	1.9	0.014	GC-MS
$\gamma$ -Tocopherol	1.8	0.032	GC-MS
RI 2438 unknown	1.7	<0.001	GC-MS
RI 1650 unknown	1.6	<0.001	GC-MS
RI 1234 unknown	1.5	0.015	GC-MS
RI 1528 unknown	1.5	<0.001	GC-MS
RI 3251 unknown	1.5	0.002	GC-MS
<b>Up-regulated metabolites</b>			
Ornithine	3.5	0.017	LC-MS
Tryptophan	1.6, 2.3	0.001, 0.001	GC-MS, LC-MS
Arginine	2.2	<0.001	LC-MS
Aspartic acid	1.7	0.016	LC-MS

#### 4. Discussion

Plants are highly responsive to the intensity, quality, and direction of light, which provides vital energy and environmental information. It is a well-known fact that red and blue light are the most effective in promoting photosynthesis [29,60–63]. There is considerable evidence, however, that green wavelengths are not only absorbed by leaf tissue, but they also regulate a number of physiological responses and anatomical features in plants [28,29,37,39,64–67].

##### 4.1. Green Light-Induced Changes in the Photosynthetic Performance of Developing Pea Cotyledons

With the modern development of LED technology, it has become possible to use light to regulate plant growth and development. Due to their ease of spectral distribution control, simple combination, lower heat emission, and longer life, LEDs are widely used as artificial light sources for indoor plant production [36,68–70]. However, there is a gap in the research investigating the effects of green LEDs on seed development. In our research, we investigated how the addition of green light to red and blue LEDs affects the photochemical activity of cotyledons in *P. sativum* seeds at the mid-maturation stage (Figure 1 and Figure S1). We recorded the time course of a Chl *a* fluorescence induction transient. The intensity of Chl *a* fluorescence increased from the initial value 'O' to the maximum value 'P', through two intermediate phases 'J' and 'I', after a pulse of actinic light. This process is known as the 'fast kinetics' of the Chl *a* fluorescence or OJIP test and is affected by the physiological state of the plant and environmental factors [71]. In our

previous study, we showed that photochemical reactions were registered in the pod, coat, and cotyledons of developing pea seeds [10,11]. The kinetics of the OJIP results was faster in cotyledons than in other plant tissues, indicating a faster reduction of the plastoquinone pool in PSII as a result of the low light intensity received during development [23]. Here, we provided a detail analysis of the OJIP kinetics using the parameters proposed by the Photon Systems Instruments protocols. The performance index, a crucial parameter in OJIP analyses, displays the changes in fluorescence due to antenna-conformation alterations and energy fluctuations [72]. In our research, adding green light to blue and red ones positively affected the performance index in PSII ( $PI_{ABS}$ ), together with the photosynthetic (Phi\_Po) and electron (Phi\_Eo) transport potentials of the reaction centers (Figure 2). Similar results were recently obtained in [27], which showed that under low light conditions, partial replacement of red by green light has beneficial effects on tomato development. Adding green light increased the photosynthetic yield, reduced energy dissipation through NPQ mechanisms, alleviated the photoreduction of the plastoquinone  $Q_A$  pool, and significantly reduced stomatal conductance and transpiration [27]. Finally, the quantum yield results for  $CO_2$  fixation showed that green light was able to efficiently drive photosynthesis.

It is well known that under low light intensities, plants increase their antenna size to capture more light energy [73]. In conditions of low light, chloroplasts can enhance the level of chlorophyll *b*, which in turn leads to an increase in the size of the peripheral light-harvesting antenna complexes [74]. Puthur et al. [4,17] proposed that seeds can also adapt to perform photochemical reactions under low light with the help of a large antenna. According to our results, the ABS/RC parameter, which correlates with the effective antenna size, was lower in cotyledons than in leaves, and lower in cotyledons developing under red–green–blue light than those under red–blue light (Figure 2). Taken together, this clearly indicates that the addition of green LEDs increased the intensity of light used by cotyledons for photochemical activity.

It has been shown that green light has the ability to penetrate the leaf and stimulate photosystems in deeper tissues, while red and blue light are more effective in the upper cell layers [32,37,75,76]. It is also known that green light, due to its high transmittance and reflectance, can penetrate deeper into the plant canopy. It can increase light interception and whole-canopy photosynthesis [37,65,73]. In addition, green light induces shade avoidance, helping to regulate plant growth and development [61]. Green light is less efficient than red light in driving photosynthesis, but it can improve the plant growth at low light levels by changing the vertical distribution of light [66]. We hypothesize that the same effects occur in pea pods. Our previous work showed that the PAR reaching the pea cotyledons has a high proportion of green light with low proportions of blue and red light [23]. Green light appears to partially compensate for the lack of blue light and the low amount of red light for seed cotyledons, increasing the flux of light energy available for photochemical processes.

#### 4.2. Green Light-Induced Metabolic Shifts in the Cotyledons of Mature Pea Seeds

The embryonic chloroplasts' primary function is to produce NADP(H) and ATP, which are used to convert sucrose coming from the mother plant into proteins, starch, and oils [10,12,14–17]. Thus, the embryonic photochemical efficiency may affect the nutrient accumulation during seed maturation. To test this assumption, we obtained mature pea seeds developed under RB and RGB light and analyzed their weight, germination capability, and amount of storage substances (proteins, starch, and oils) (Table 2). It was found that complementation of the red and blue light with green light resulted in an increase in the seed weights. Pea seeds are an important source of protein for human nutrition, with an average protein content of 20–25% of the dry weight [77]. Notably, the pea cotyledons developed in the RGB module contained  $22 \pm 0.6\%$  (DW) protein, compared to  $19 \pm 0.2\%$  in pea cotyledons developed in the RB module.

Thus, we discovered that modulation of the light spectrum mostly affects the nutritional value of seeds (Table 2). To address the potential metabolic pathways underlying this phenomenon, the biochemical composition of the cotyledons isolated from mature pea



seeds was determined. The difference in metabolic patterns between seeds developed in the RB and RGB modules was considerable, which was confirmed by the PCA analysis (Figure 3). The PCA score plot showed a significant difference in the inter-group variance between these two groups, with a higher variability in the biochemical composition of the cotyledons developed under RGB light.

Surprisingly, the relative abundance of the majority of the annotated metabolites in the cotyledons of seeds developed under RGB light were 3.4–7.6 times lower than those grown under RB light (Table 3). The most responsive metabolites were intermediates of the main synthetic and energetic pathways (glycolysis, TCA cycle, and pentose phosphate pathway). This could be the result of a redirection of carbon flow. The additional energy (NADPH and ATP) provided by the enhanced embryonic photosynthesis can be redirected to the glycolytic pathway instead of the Calvin cycle, as it is in leaves [18]. Intermediates and products of the glycolytic pathway, such as phosphoenolpyruvate (PEP) and pyruvate, are further involved in fatty acid synthesis and in the anaplerotic pathway [78]. It has been shown that phosphoenolpyruvate carboxylase (PEPC) is highly active in maturing seeds [79–81]. PEPC can direct PEP, pyruvate, and TCA intermediates, via malate and oxaloacetate, into the amino acid synthesis pathway [78]. The synthesized amino acids can be used in the biosynthesis of storage proteins.

Meanwhile, four amino acids, ornithine, tryptophan, arginine, and aspartic acid, were significantly up-regulated ( $p \leq 0.02$ ,  $FC \geq 1.7$ ). Several differentially abundant metabolites are involved in the ornithine cycle and polyamine (PA) biosynthetic pathway (Figure 4). Among them, arginine is the most suitable storage form of organic nitrogen due to its high nitrogen-to-carbon ratio. Furthermore, arginine serves as a precursor in the synthesis of the secondary messenger NO [82].

Polyamine levels are known to increase during the initial stages of embryo development, as they are important for cell proliferation and differentiation [83,84]. What is the explanation for the regulatory effect of green light on PA levels in pea seeds in our experiments? Primarily, light appears to affect PA biosynthesis [85–87]. The link between PAs and photosynthesis is suggested by the high levels of putrescine, spermidine, and spermine in thylakoid membranes and light-harvesting complex II, whereas the reaction center of PSII is rich in spermine [88–90]. It has also been shown that the activities of arginine decarboxylase, ornithine decarboxylase, SPd synthase, and SPm synthase are altered under different light conditions [91,92]. Chloroplasts contain highly active PA enzymes and transglutaminase, which catalyze the covalent binding of polyamines to proteins [87,93,94].

According to Pál et al. [86], plants maintain the optimal concentrations and ratios of PAs under different spectral compositions of light. Some authors suggested that the amount of light and the duration of illumination may affect the PA pool in plant cells more than the light quality [85,91,95]. Gondor et al. [85] showed that light, on the one hand, regulates the level of endogenous putrescine in wheat leaves and, on the other hand, exogenous PAs can improve photosynthesis under lower light conditions. Zhang et al. [96] found that exogenous polyamines can improve the photosynthesis in salt-stressed cucumber seedlings by increasing the photochemical efficiency of PSII. Ioannidis and Kotzabasis [97] emphasized the importance of chloroplast polyamines for photosynthetic membrane functionality. The study showed that putrescine efficiently stimulates ATP synthesis, while spermidine and spermine improve non-photochemical quenching. The mechanism of action of PAs probably involves their direct binding to the extrinsic proteins and the hydrophilic domains of the intrinsic polypeptides of photosystem II. PAs act through electrostatic interaction due to their polycationic properties, and the polycationic selectivity effect in decreasing order is  $\text{Spm}^{4+} > \text{Spd}^{3+} > \text{Put}^{2+}$  [87]. This electrostatic interaction could provide some stability to the conformation of thylakoid proteins, and thus help to maintain photosynthetic activity.

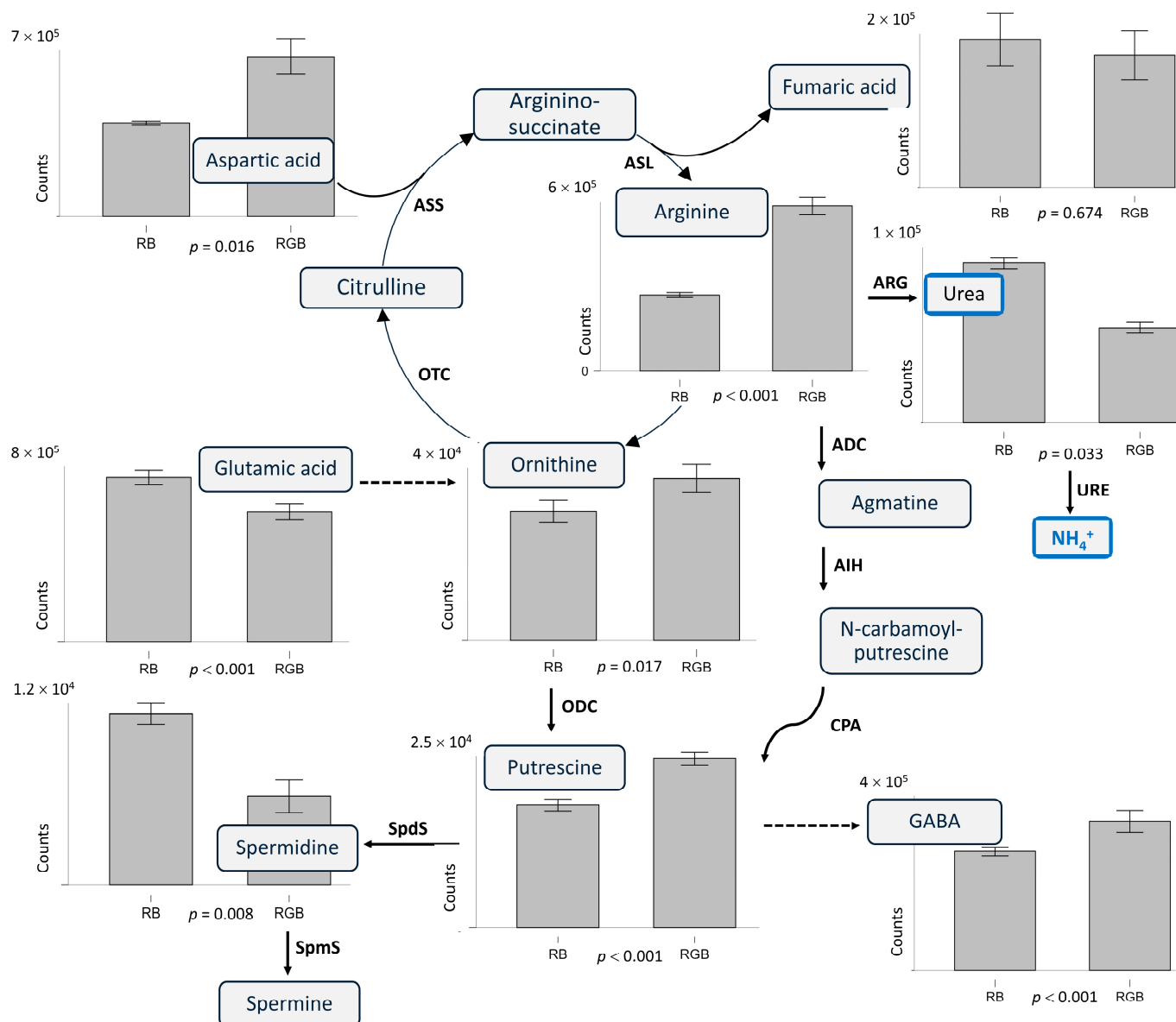


**Figure 4.** The ornithine–urea cycle and polyamine biosynthesis pathway with changes in metabolite levels in cotyledons of mature pea seeds developed under RB (red–blue) and RGB (red–green–blue) light. All values are presented as intensities (counts) corresponding to the peak areas of extracted ion chromatograms (Tables S4 and S5). Bars represent the mean  $\pm$  SE. Direct reactions are presented as straight lines and reactions involving several steps are presented as dashed lines. ADC—arginine decarboxylase; AIH—agmatine iminohydrolase; ARG—arginase; ASL—argininosuccinate lyase; ASS—argininosuccinate synthase; GABA— $\gamma$ -aminobutyric acid; NCPAH—N-carbamoyl-putrescine amidohydrolase; ODC—ornithine decarboxylase; SpdS—spermidine synthase; SpmS—spermine synthase; URE—urease.

## 5. Conclusions

In addition to leaves, photosynthesis can occur in other green plant organs, including developing seeds of many crops. However, the mechanisms of embryonic photosynthesis and how seed embryos receive sufficient light for photochemical reactions remain unclear. It is widely acknowledged that chlorophylls and carotenoids are capable of absorbing light within the blue and red spectral regions. Meanwhile, many studies have shown that green light excites photosystems in leaves of shade-grown plants and deeper tissues of leaves. In this work, we grew *P. sativum* plants under red–blue and red–green–blue

LEDs and showed that green light had a favorable impact on seed maturation. Mature seeds developed under green light had a significantly higher weight and contained more proteins. Further, we recorded the time course of the Chl *a* fluorescence induction transient in the cotyledons of pea seeds at the photochemically active middle stage of maturation, which is characterized by the active synthesis of storage substances. The data showed an increase in the photosynthetic performance index (PIABS), quantum yield of primary photochemistry (PHI<sub>Po</sub>), and electron transport potential of the active reaction centers (PHI<sub>Eo</sub>) in cotyledons of seeds matured under the green light. The metabolomics analysis using GC-MS and RP-UHPLC-MS revealed significant biochemical differences between seeds developed in the RB and RGB modules. Cotyledons developed under green light had significantly lower levels of organic acids of the TCA cycle, carbohydrates, nucleotide monophosphates, and nitrogenous substances such as uric acid and spermidine. This could be due to the accelerated synthesis of reserve compounds. However, four amino acids, ornithine, tryptophan, arginine, and aspartic acid, were significantly up-regulated. These metabolites are involved in the pathways of the ornithine–urea cycle and polyamine biosynthesis. Among the proteinogenic amino acids, arginine has the highest nitrogen-to-carbon ratio, which makes it especially suitable as a storage form of organic nitrogen. Our data show the role of green light in embryonic photosynthesis, suggesting a link between embryonic photochemical activity and the biochemical composition of seeds. Further studies on a broader range of crops supplemented with different light spectra, followed by analysis of their photochemical activity and specific metabolic pathways, could provide valuable insights for the next generation of research.

**Supplementary Materials:** The following supporting information can be downloaded at: <https://www.mdpi.com/article/10.3390/agronomy14102367/s1>, Figure S1: Close-type installation for growing the *P. sativum* plants; Figure S2: Sample scores for the first two principal components derived from PCA of the thermostable and thermolabile polar metabolite profiles of *P. sativum* cotyledons developed under RB or RGB light and quality control samples; Figure S3: Volcano plot showing the metabolites of *P. sativum* cotyledons developed under RB or RGB light; Figure S4: Heatmap showing the metabolite profiles of *P. sativum* cotyledons developed under RB or RGB light; Table S1: Gas chromatography and electron ionization–quadrupole mass spectrometry settings used for the analysis of primary polar thermally stable metabolites extracted from *P. sativum* cotyledons; Table S2: Composition of the alkane standard mixture used to determine Kovats retention time indices (RIs); Table S3: Ion pair-reversed phase ultra-high performance liquid chromatography separation conditions and electrospray ionization–triple quadrupole tandem mass spectrometry settings used for the analysis of anionic primary thermolabile metabolites extracted from *P. sativum* cotyledons; Table S4: Thermostable metabolites detected by GC-MS analysis in methanol/water extracts of *P. sativum* cotyledons developed under RB or RGB light; Table S5: Thermolabile polar metabolites detected by targeted UHPLC-MS analysis of the ethanol/water extracts of *P. sativum* cotyledons developed under RB or RGB light.

**Author Contributions:** Conceptualization, G.S.; Methodology, A.K., A.F. and G.S.; Software, N.F. and T.B.; Validation, S.M.; Formal analysis, N.S., E.T., A.S. (Alena Soboleva), A.O., A.B. and A.S. (Anastasia Smolenskaya); Investigation, N.S., A.S. (Alena Soboleva), A.O., A.B., A.S. (Anastasia Smolenskaya) and N.F.; Resources, A.K. and A.F.; Data curation, N.F. and T.B.; Writing—original draft, N.S., E.T. and G.S.; Writing—review and editing, A.K., A.F., S.M. and G.S.; Visualization, E.T. and T.B.; Supervision, G.S.; Funding acquisition, S.M. All authors have read and agreed to the published version of the manuscript.

**Funding:** This research was funded by the Russian Science Foundation, grant no. 20-16-00086.

**Data Availability Statement:** Data are contained within the article and Supplementary Materials.

**Acknowledgments:** The infrastructural support from the Ministry of Science and Higher Education of the Russian Federation (theme #122042700043-9) is acknowledged.

**Conflicts of Interest:** The authors declare no conflicts of interest.

## References

1. Brazel, A.J.; Ó'Maoiléidigh, D.S. Photosynthetic activity of reproductive organs. *J. Exp. Bot.* **2019**, *70*, 1737–1754. [[CrossRef](#)] [[PubMed](#)]
2. Henry, R.J.; Furtado, A.; Rangan, P. Pathways of photosynthesis in non-leaf tissues. *Biology* **2020**, *9*, 438. [[CrossRef](#)]
3. Simkin, A.J.; Faralli, M.; Ramamoorthy, S.; Lawson, T. Photosynthesis in non-foliar tissues: Implications for yield. *Plant J.* **2019**, *101*, 1001–1015. [[CrossRef](#)] [[PubMed](#)]
4. Puthur, J.T.; Shackira, A.M.; Saradhi, P.P.; Bartels, D. Chloroembryos: A unique photosynthesis system. *J. Plant Physiol.* **2013**, *170*, 1131–1138. [[CrossRef](#)]
5. Smolikova, G.N.; Medvedev, S.S. Photosynthesis in the seeds of chloroembryophytes. *Russ. J. Plant Physiol.* **2016**, *63*, 1–12. [[CrossRef](#)]
6. Cho, Y.B.; Stutz, S.S.; Jones, S.I.; Wang, Y.; Pelech, E.A.; Ort, D.R. Impact of pod and seed photosynthesis on seed filling and canopy carbon gain in soybean. *Plant Physiol.* **2023**, *193*, 966–979. [[CrossRef](#)]
7. Sela, A.; Piskurewicz, U.; Megies, C.; Mène-Saffrané, L.; Finazzi, G.; Lopez-Molina, L. Embryonic photosynthesis affects post-germination plant growth. *Plant Physiol.* **2020**, *182*, 2166–2181. [[CrossRef](#)]
8. Periasamy, K.; Vivekandan, M. Photosynthesis in the Chloroembryo of *Cyamopsis tetragonoloba* Taub. *Ann. Bot.* **1981**, *47*, 793–797. [[CrossRef](#)]
9. Puthur, J.T.; Pardha Saradhi, P. Developing embryos of *Sesbania sesban* have unique potential to photosynthesize under high osmotic environment. *J. Plant Physiol.* **2004**, *161*, 1107–1118. [[CrossRef](#)]
10. Smolikova, G.; Kreslavski, V.; Shiroglazova, O.; Bilova, T.; Sharova, E.; Frolov, A.; Medvedev, S. Photochemical activity changes accompanying the embryogenesis of pea (*Pisum sativum*) with yellow and green cotyledons. *Funct. Plant Biol.* **2018**, *45*, 228. [[CrossRef](#)]
11. Smolikova, G.; Shiroglazova, O.; Vinogradova, G.; Leppyanen, I.; Dinastiya, E.; Yakovleva, O.; Dolgikh, E.; Titova, G.; Frolov, A.; Medvedev, S. Comparative analysis of the plastid conversion, photochemical activity and chlorophyll degradation in developing embryos of green-seeded and yellow-seeded pea (*Pisum sativum*) cultivars. *Funct. Plant Biol.* **2020**, *47*, 409–424. [[CrossRef](#)] [[PubMed](#)]
12. Ruuska, S.A.; Schwender, J.; Ohlrogge, J.B. The capacity of green oilseeds to utilize photosynthesis to drive biosynthetic processes. *Plant Physiol.* **2004**, *136*, 2700–2709. [[CrossRef](#)]
13. Smolikova, G.N.; Medvedev, S.S. Seed carotenoids: synthesis, diversity, and functions. *Russ. J. Plant Physiol.* **2015**, *62*, 1–13. [[CrossRef](#)]
14. Borisjuk, L.; Nguyen, T.H.; Neuberger, T.; Rutten, T.; Tschiersch, H.; Claus, B.; Feussner, I.; Webb, A.G.; Jakob, P.; Weber, H.; et al. Gradients of lipid storage, photosynthesis and plastid differentiation in developing soybean seeds. *New Phytol.* **2005**, *167*, 761–776. [[CrossRef](#)] [[PubMed](#)]
15. Wu, X.L.; Liu, Z.H.; Hu, Z.H.; Huang, R.Z. BnWRI1 coordinates fatty acid biosynthesis and photosynthesis pathways during oil accumulation in rapeseed. *J. Integr. Plant Biol.* **2014**, *56*, 582–593. [[CrossRef](#)] [[PubMed](#)]
16. Alloreant, G.; Osorio, S.; Ly Vu, J.; Falconet, D.; Jouhet, J.; Kuntz, M.; Fernie, A.R.; Lerbs-Mache, S.; Macherel, D.; Courtois, F.; et al. Adjustments of embryonic photosynthetic activity modulate seed fitness in *Arabidopsis thaliana*. *New Phytol.* **2015**, *205*, 707–719. [[CrossRef](#)] [[PubMed](#)]
17. Shackira, A.M.; Sarath, N.G.; Aswathi, K.P.R.; Pardha-Saradhi, P.; Puthur, J.T. Green seed photosynthesis: What is it? What do we know about it? Where to go? *Plant Physiol. Rep.* **2022**, *27*, 573–579. [[CrossRef](#)]
18. Schwender, J.; Goffman, F.; Ohlrogge, J.B.; Shachar-Hill, Y. Rubisco without the Calvin cycle improves the carbon efficiency of developing green seeds. *Nature* **2004**, *432*, 779–782. [[CrossRef](#)]
19. Weber, H.; Borisjuk, L.; Wobus, U. Molecular physiology of legume seed development. *Annu. Rev. Plant Biol.* **2005**, *56*, 253–279. [[CrossRef](#)]
20. Allen, D.K.; Ohlrogge, J.B.; Shachar-Hill, Y. The role of light in soybean seed filling metabolism. *Plant J.* **2009**, *58*, 220–234. [[CrossRef](#)] [[PubMed](#)]
21. Borisjuk, L.; Rolletschek, H. The oxygen status of the developing seed. *New Phytol.* **2009**, *182*, 17–30. [[CrossRef](#)] [[PubMed](#)]
22. Tschiersch, H.; Borisjuk, L.; Rutten, T.; Rolletschek, H. Gradients of seed photosynthesis and its role for oxygen balancing. *BioSystems* **2011**, *103*, 302–308. [[CrossRef](#)] [[PubMed](#)]
23. Smolikova, G.N.; Stepanova, N.V.; Kamionskaya, A.M.; Medvedev, S.S. Photochemical activity in developing pea (*Pisum sativum* L.) cotyledons depends on the light transmittance of covering tissues and the spectral composition of light. *Vavilov J. Genet. Breed.* **2023**, *27*, 980–987. [[CrossRef](#)] [[PubMed](#)]
24. Went, F.W. *The Experimental Control of Plant Growth*; Chronica Botanica Co.: Waltham, MA, USA, 1957.
25. Golovatskaya, I.F.; Karnachuk, R.A. Role of green light in physiological activity of plants. *Russ. J. Plant Physiol.* **2015**, *62*, 727–740. [[CrossRef](#)]
26. Smith, H.L.; McAusland, L.; Murchie, E.H. Don't ignore the green light: Exploring diverse roles in plant processes. *J. Exp. Bot.* **2017**, *68*, 2099–2110. [[CrossRef](#)] [[PubMed](#)]
27. Trojak, M.; Skowron, E.; Sobala, T.; Kocurek, M.; Palyga, J. Effects of partial replacement of red by green light in the growth spectrum on photomorphogenesis and photosynthesis in tomato plants. *Photosynth. Res.* **2022**, *151*, 295–312. [[CrossRef](#)]

28. Lv, X.; Gao, S.; Li, N.; Lv, Y.; Chen, Z.; Cao, B.; Xu, K. Comprehensive insights into the influence of supplemental green light on the photosynthesis of ginger (*Zingiber officinale* Roscoe). *Protoplasma* **2022**, *259*, 1477–1491. [[CrossRef](#)]
29. Liu, J.; van Iersel, M.W. Photosynthetic physiology of blue, green, and red light: Light intensity effects and underlying mechanisms. *Front. Plant Sci.* **2021**, *12*, 619987. [[CrossRef](#)]
30. Sierra, J.; Escobar-Tovar, L.; Leon, P. Plastids: Diving into their diversity, their functions, and their role in plant development. *J. Exp. Bot.* **2023**, *74*, 2508–2526. [[CrossRef](#)]
31. Terashima, I.; Hanba, Y.T.; Tholen, D.; Niinemets, Ü. Leaf functional anatomy in relation to photosynthesis. *Plant Physiol.* **2011**, *155*, 108–116. [[CrossRef](#)]
32. Brodersen, C.R.; Vogelmann, T.C. Do changes in light direction affect absorption profiles in leaves? *Funct. Plant Biol.* **2010**, *37*, 403. [[CrossRef](#)]
33. Kim, H.-H.; Goins, G.D.; Wheeler, R.M.; Sager, J.C. Green-light supplementation for enhanced lettuce growth under red- and blue-light-emitting diodes. *HortScience* **2004**, *39*, 1617–1622. [[CrossRef](#)] [[PubMed](#)]
34. Kong, S.-W.; Chung, H.-Y.; Chang, M.-Y.; Fang, W. The contribution of different spectral sections to increase fresh weight of Boston lettuce. *HortScience* **2015**, *50*, 1006–1010. [[CrossRef](#)]
35. Bian, Z.-H.; Cheng, R.-F.; Yang, Q.-C.; Wang, J.; Lu, C. Continuous light from red, blue, and green light-emitting diodes reduces nitrate content and enhances phytochemical concentrations and antioxidant capacity in lettuce. *J. Am. Soc. Hortic. Sci.* **2016**, *141*, 186–195. [[CrossRef](#)]
36. Zakurin, A.O.; Shchennikova, A.V.; Kamionskaya, A.M. Artificial-light culture in protected ground plant growing: Photosynthesis, photomorphogenesis, and prospects of LED application. *Russ. J. Plant Physiol.* **2020**, *67*, 413–424. [[CrossRef](#)]
37. Terashima, I.; Fujita, T.; Inoue, T.; Chow, W.S.; Oguchi, R. Green light drives leaf photosynthesis more efficiently than red light in strong white light: Revisiting the enigmatic question of why leaves are green. *Plant Cell Physiol.* **2009**, *50*, 684–697. [[CrossRef](#)]
38. Liu, H.; Fu, Y.; Wang, M.; Liu, H. Green light enhances growth, photosynthetic pigments and CO<sub>2</sub> assimilation efficiency of lettuce as revealed by “knock out” of the 480–560 nm spectral waveband. *Photosynthetica* **2017**, *55*, 144–152. [[CrossRef](#)]
39. Bian, Z.; Yang, Q.; Li, T.; Cheng, R.; Barnett, Y.; Lu, C. Study of the beneficial effects of green light on lettuce grown under short-term continuous red and blue light-emitting diodes. *Physiol. Plant.* **2018**, *164*, 226–240. [[CrossRef](#)]
40. Muneer, S.; Kim, E.; Park, J.; Lee, J. Influence of green, red and blue light emitting diodes on multiprotein complex proteins and photosynthetic activity under different light intensities in lettuce leaves (*Lactuca sativa* L.). *Int. J. Mol. Sci.* **2014**, *15*, 4657–4670. [[CrossRef](#)]
41. Claypool, N.B.; Lieth, J.H. Green light improves photosystem stoichiometry in *Cucumber* seedlings (*Cucumis sativus*) compared to monochromatic red light. *Plants* **2021**, *10*, 824. [[CrossRef](#)]
42. Ma, Y.; Hu, L.; Wu, Y.; Tang, Z.; Xiao, X.; Lyu, J.; Xie, J.; Yu, J. Green light partial replacement of red and blue light improved drought tolerance by regulating water use efficiency in *Cucumber* seedlings. *Front. Plant Sci.* **2022**, *13*, 878932. [[CrossRef](#)] [[PubMed](#)]
43. Kasajima, S.; Inoue, N.; Mahmud, R.; Kato, M. Developmental responses of wheat cv. Norin 61 to fluence rate of green light. *Plant Prod. Sci.* **2008**, *11*, 76–81. [[CrossRef](#)]
44. Park, B.G.; Lee, J.H.; Shin, E.J.; Kim, E.A.; Nam, S.Y. Light quality influence on growth performance and physiological activity of *Coleus* cultivars. *Int. J. Plant Biol.* **2024**, *15*, 807–826. [[CrossRef](#)]
45. Smýkal, P.; Aubert, G.; Burstin, J.; Coyne, C.J.; Ellis, N.T.H.; Flavell, A.J.; Ford, R.; Hýbl, M.; Macas, J.; Neumann, P.; et al. Pea (*Pisum sativum* L.) in the Genomic Era. *Agronomy* **2012**, *2*, 74–115. [[CrossRef](#)]
46. Mamontova, T.; Lukasheva, E.; Mavropolo-Stolyarenko, G.; Proksch, C.; Bilova, T.; Kim, A.; Babakov, V.; Grishina, T.; Hoehnwarter, W.; Medvedev, S.; et al. Proteome map of pea (*Pisum sativum* L.) embryos containing different amounts of residual chlorophylls. *Int. J. Mol. Sci.* **2018**, *19*, 4066. [[CrossRef](#)]
47. Coolbear, P.; Francis, A.; Grienson, D. The effect of low temperature pre-Sowing treatment on the germination performance and membrane integrity of artificially aged tomato seeds. *J. Exp. Bot.* **1984**, *35*, 1609–1617. [[CrossRef](#)]
48. International Seed Testing Association. *International Rules for Seed Testing*; International Seed Testing Association: Basserdorf, Switzerland, 2009; ISSN 2310-3655.
49. Don, R. *ISTA Handbook on Seedling Evaluation*, 3rd ed.; The International Seed Testing Association: Basserdorf, Switzerland, 2003; ISBN 3-906549-39-9.
50. Ermakov, A.I.; Arasimovich, V.V.; Smirnova-Ikonnikova, M.I.; Yarosh, N.P.; Lukovnikova, G.A. *Methods for the Biochemical Analysis of Plants*, 3rd ed.; Agropromizdat: Leningrad, Russia, 1987.
51. Sáez-Plaza, P.; Navas, M.J.; Wybraniec, S.; Michałowski, T.; Asuero, A.G. An overview of the Kjeldahl method of nitrogen determination. Part II. sample preparation, working scale, instrumental finish, and quality control. *Crit. Rev. Anal. Chem.* **2013**, *43*, 224–272. [[CrossRef](#)]
52. Photon Systems Instruments. *Manual and User Guide*; Photon Systems Instruments: Drásov, Czech Republic, 2018.
53. Strasser, R.J.; Srivastava, A.; Tsimilli-Michael, M. The Fluorescence Transient as a Tool to Characterize and Screen Photosynthetic Samples. In *Probing Photosynthesis: Mechanism, Regulation and Adaptation*; Yunus, M., Pathre, U., Mohanty, P., Eds.; Taylor and Francis: Oxfordshire, UK, 2000; pp. 445–483.



54. Leonova, T.; Popova, V.; Tsarev, A.; Henning, C.; Antonova, K.; Rogovskaya, N.; Vikhnina, M.; Baldensperger, T.; Soboleva, A.; Dinastia, E.; et al. Does protein glycation impact on the drought-related changes in metabolism and nutritional properties of mature pea (*Pisum sativum* L.) seeds? *Int. J. Mol. Sci.* **2020**, *21*, 567. [[CrossRef](#)]
55. Chantseva, V.; Bilova, T.; Smolikova, G.; Frolov, A.; Medvedev, S. 3D-clinorotation induces specific alterations in metabolite profiles of germinating *Brassica napus* L. seeds. *Biol. Commun.* **2019**, *64*, 55–74. [[CrossRef](#)]
56. Shumilina, J.; Kiryushkin, A.S.; Frolova, N.; Mashkina, V.; Ilina, E.L.; Puchkova, V.A.; Danko, K.; Silinskaya, S.; Serebryakov, E.B.; Soboleva, A.; et al. Integrative proteomics and metabolomics analysis reveals the role of small signaling peptide rapid alkalization factor 34 (RALF34) in cucumber roots. *Int. J. Mol. Sci.* **2023**, *24*, 7654. [[CrossRef](#)]
57. Benjamini, Y.; Hochberg, Y. Controlling the false discovery rate: A practical and powerful approach to multiple testing. *J. R. Stat. Soc. Ser. B* **1995**, *57*, 289–300. [[CrossRef](#)]
58. Silverman, B.W. *Density Estimation for Statistics and Data Analysis*; Routledge: New York, NY, USA, 1986; ISBN 9780412246203.
59. Harvey, D.J.; Vouros, P. Mass spectrometric fragmentation of trimethylsilyl and related alkylsilyl derivatives. *Mass Spectrom. Rev.* **2020**, *39*, 105–211. [[CrossRef](#)] [[PubMed](#)]
60. Bouly, J.-P.; Schleicher, E.; Dionisio-Sese, M.; Vandenbussche, F.; Van Der Straeten, D.; Bakrim, N.; Meier, S.; Batschauer, A.; Galland, P.; Bittl, R.; et al. Cryptochrome blue light photoreceptors are activated through interconversion of flavin redox states. *J. Biol. Chem.* **2007**, *282*, 9383–9391. [[CrossRef](#)] [[PubMed](#)]
61. Johkan, M.; Shoji, K.; Goto, F.; Hahida, S.; Yoshihara, T. Effect of green light wavelength and intensity on photomorphogenesis and photosynthesis in *Lactuca sativa*. *Environ. Exp. Bot.* **2012**, *75*, 128–133. [[CrossRef](#)]
62. Bantis, F.; Smirnakou, S.; Ouzounis, T.; Koukounaras, A.; Ntagkas, N.; Radoglou, K. Current status and recent achievements in the field of horticulture with the use of light-emitting diodes (LEDs). *Sci. Hortic.* **2018**, *235*, 437–451. [[CrossRef](#)]
63. Gao, W.; Chen, F.; Yan, W.; Wang, Z.; Zhang, G.; Ren, Z.; Cao, H.; Sun, Z. Toward green manufacturing evaluation of light-emitting diodes (LED) production—A case study in China. *J. Clean. Prod.* **2022**, *368*, 133149. [[CrossRef](#)]
64. Battle, M.W.; Jones, M.A. Cryptochromes integrate green light signals into the circadian system. *Plant. Cell Environ.* **2020**, *43*, 16–27. [[CrossRef](#)]
65. Dou, H.; Niu, G.; Gu, M. Photosynthesis, morphology, yield, and phytochemical accumulation in basil plants influenced by substituting green light for partial red and/or blue light. *HortScience* **2019**, *54*, 1769–1776. [[CrossRef](#)]
66. Kaiser, E.; Weerheim, K.; Schipper, R.; Dieleman, J.A. Partial replacement of red and blue by green light increases biomass and yield in tomato. *Sci. Hortic.* **2019**, *249*, 271–279. [[CrossRef](#)]
67. Snowden, M.C.; Cope, K.R.; Bugbee, B. Sensitivity of seven diverse species to blue and green light: Interactions with photon flux. *PLoS ONE* **2016**, *11*, e0163121. [[CrossRef](#)]
68. Winnacker, A. Light Emitting Diodes (LEDs). In *The Physics Behind Semiconductor Technology*; Springer International Publishing: Cham, Switzerland, 2022; pp. 159–178.
69. Dutta Gupta, S.; Agarwal, A. Artificial lighting system for plant growth and development: Chronological advancement, working principles, and comparative assessment. In *Light Emitting Diodes for Agriculture*; Dutta Gupta, S., Ed.; Springer: Singapore, 2017; pp. 1–25. ISBN 978-981-10-5807-3.
70. Shin, E.J.; Lee, J.H.; Nam, S.Y. Changes in growth, visual qualities, and photosynthetic parameters in *Peperomia* species and cultivars under different color temperatures of white lighting conditions. *J. Agric. Life Environ. Sci.* **2023**, *35*, 307–321. [[CrossRef](#)]
71. Guidi, L.; Lo Piccolo, E.; Landi, M. Chlorophyll fluorescence, photoinhibition and abiotic stress: Does it make any difference the fact to be a C3 or C4 species? *Front. Plant Sci.* **2019**, *10*, 174. [[CrossRef](#)]
72. Kumar, D.; Singh, H.; Raj, S.; Soni, V. Chlorophyll *a* fluorescence kinetics of mung bean (*Vigna radiata* L.) grown under artificial continuous light. *Biochem. Biophys. Rep.* **2020**, *24*, 100813. [[CrossRef](#)]
73. Abhijita, S.; Dalal, V.K.; Misra, A.N. The Effect of Light Quality and Quantity on Photosynthesis. In *A Closer Look at Photosynthesis*; Dalal, V.K., Misra, A.N., Eds.; Nova Science Publishers, Inc.: New York, NY, USA, 2023; ISBN 979-8-88697-815-5.
74. Wu, G.; Ma, L.; Sayre, R.T.; Lee, C.-H. Identification of the optimal light harvesting antenna size for high-light stress mitigation in plants. *Front. Plant Sci.* **2020**, *11*, 505. [[CrossRef](#)]
75. Nishio, J.N. Why are higher plants green? Evolution of the higher plant photosynthetic pigment complement. *Plant. Cell Environ.* **2000**, *23*, 539–548. [[CrossRef](#)]
76. Vogelmann, T.C.; Evans, J.R. Profiles of light absorption and chlorophyll within spinach leaves from chlorophyll fluorescence. *Plant. Cell Environ.* **2002**, *25*, 1313–1323. [[CrossRef](#)]
77. Shen, Y.; Hong, S.; Li, Y. Pea protein composition, functionality, modification, and food applications: A review. *Adv. Food Nutr. Res.* **2022**, *101*, 71–127.
78. Yang, J.; Kalhan, S.C.; Hanson, R.W. What is the metabolic role of phosphoenolpyruvate carboxykinase? *J. Biol. Chem.* **2009**, *284*, 27025–27029. [[CrossRef](#)]
79. Feria, A.-B.; Alvarez, R.; Cochereau, L.; Vidal, J.; García-Mauriño, S.; Echevarría, C. Regulation of phosphoenol pyruvate carboxylase phosphorylation by metabolites and abscisic acid during the development and germination of barley seeds. *Plant Physiol.* **2008**, *148*, 761–774. [[CrossRef](#)]
80. King, S.P.; Badger, M.R.; Furbank, R.T. CO<sub>2</sub> refixation characteristics of developing canola seeds and silique wall. *Aust. J. Plant Physiol.* **1998**, *25*, 377. [[CrossRef](#)]

81. Černý, M.; Doubnerová, V.; Müller, K.; Ryšlavá, H. Characterization of phosphoenolpyruvate carboxylase from mature maize seeds: Properties of phosphorylated and dephosphorylated forms. *Biochimie* **2010**, *92*, 1362–1370. [[CrossRef](#)] [[PubMed](#)]
82. Winter, G.; Todd, C.D.; Trovato, M.; Forlani, G.; Funck, D. Physiological implications of arginine metabolism in plants. *Front. Plant Sci.* **2015**, *6*, 534. [[CrossRef](#)]
83. Chen, D.; Shao, Q.; Yin, L.; Younis, A.; Zheng, B. Polyamine function in plants: Metabolism, regulation on development, and roles in abiotic stress responses. *Front. Plant Sci.* **2019**, *9*, 1945. [[CrossRef](#)] [[PubMed](#)]
84. Blázquez, M.A. Polyamines: Their role in plant development and stress. *Annu. Rev. Plant Biol.* **2024**, *75*, 95–117. [[CrossRef](#)] [[PubMed](#)]
85. Gondor, O.K.; Tajti, J.; Hamow, K.Á.; Majláth, I.; Szalai, G.; Janda, T.; Pál, M. Polyamine metabolism under different light regimes in wheat. *Int. J. Mol. Sci.* **2021**, *22*, 11717. [[CrossRef](#)]
86. Pál, M.; Hamow, K.Á.; Rahman, A.; Majláth, I.; Tajti, J.; Gondor, O.K.; Ahres, M.; Gholizadeh, F.; Szalai, G.; Janda, T. Light Spectral composition modifies polyamine metabolism in young wheat plants. *Int. J. Mol. Sci.* **2022**, *23*, 8394. [[CrossRef](#)]
87. Shu, S.; Guo, S.-R.; Yu, L.-Y. A review: Polyamines and photosynthesis. In *Advances in Photosynthesis—Fundamental Aspects*; Najafpour, M.M., Ed.; InTech: Rijeka, Croatia, 2012.
88. Kotzabasis, K.; Fotinou, C.; Roubelakis-Angelakis, K.A.; Ghanotakis, D. Polyamines in the photosynthetic apparatus. *Photosynth. Res.* **1993**, *38*, 83–88. [[CrossRef](#)] [[PubMed](#)]
89. Navakoudis, E.; Vrentzou, K.; Kotzabasis, K. A polyamine- and LHCII protease activity-based mechanism regulates the plasticity and adaptation status of the photosynthetic apparatus. *Biochim. Biophys. Acta Bioenerg.* **2007**, *1767*, 261–271. [[CrossRef](#)] [[PubMed](#)]
90. Demetriou, G.; Neonaki, C.; Navakoudis, E.; Kotzabasis, K. Salt stress impact on the molecular structure and function of the photosynthetic apparatus—The protective role of polyamines. *Biochim. Biophys. Acta Bioenerg.* **2007**, *1767*, 272–280. [[CrossRef](#)]
91. Takács, Z.; Poór, P.; Tari, I. Comparison of polyamine metabolism in tomato plants exposed to different concentrations of salicylic acid under light or dark conditions. *Plant Physiol. Biochem.* **2016**, *108*, 266–278. [[CrossRef](#)] [[PubMed](#)]
92. Lv, Y.; Shao, G.; Jiao, G.; Sheng, Z.; Xie, L.; Hu, S.; Tang, S.; Wei, X.; Hu, P. Targeted mutagenesis of Polyamine Oxidase 5 that negatively regulates mesocotyl elongation enables the generation of direct-seeding rice with improved grain yield. *Mol. Plant* **2021**, *14*, 344–351. [[CrossRef](#)] [[PubMed](#)]
93. Andreadakis, A.; Kotzabasis, K. Changes in the biosynthesis and catabolism of polyamines in isolated plastids during chloroplast photodevelopment. *J. Photochem. Photobiol. B Biol.* **1996**, *33*, 163–170. [[CrossRef](#)]
94. Della Mea, M.; Di Sandro, A.; Dondini, L.; Del Duca, S.; Vantini, F.; Bergamini, C.; Bassi, R.; Serafini-Fracassini, D. A Zea mays 39-kDa thylakoid transglutaminase catalyses the modification by polyamines of light-harvesting complex II in a light-dependent way. *Planta* **2004**, *219*, 754–764. [[CrossRef](#)] [[PubMed](#)]
95. Toldi, D.; Gyugos, M.; Darkó, É.; Szalai, G.; Gulyás, Z.; Gierczik, K.; Székely, A.; Boldizsár, Á.; Galiba, G.; Müller, M.; et al. Light intensity and spectrum affect metabolism of glutathione and amino acids at transcriptional level. *PLoS ONE* **2019**, *14*, e0227271. [[CrossRef](#)]
96. Zhang, R.H.; Li, J.; Guo, S.R.; Tezuka, T. Effects of exogenous putrescine on gas-exchange characteristics and chlorophyll fluorescence of NaCl-stressed cucumber seedlings. *Photosynth. Res.* **2009**, *100*, 155–162. [[CrossRef](#)] [[PubMed](#)]
97. Ioannidis, N.E.; Kotzabasis, K. Effects of polyamines on the functionality of photosynthetic membrane in vivo and in vitro. *Biochim. Biophys. Acta Bioenerg.* **2007**, *1767*, 1372–1382. [[CrossRef](#)] [[PubMed](#)]

**Disclaimer/Publisher’s Note:** The statements, opinions and data contained in all publications are solely those of the individual author(s) and contributor(s) and not of MDPI and/or the editor(s). MDPI and/or the editor(s) disclaim responsibility for any injury to people or property resulting from any ideas, methods, instructions or products referred to in the content.